UC Riverside

UC Riverside Previously Published Works

Title

HYDRUS simulations of the effects of dual-drip subsurface irrigation and a physical barrier on water movement and solute transport in soils

Permalink

https://escholarship.org/uc/item/0817k6hj

Journal

Irrigation Science, 32(2)

ISSN

0342-7188

Authors

El-Nesr, Mohammad N
Alazba, AA
Šimůnek, Jiří

Publication Date

2014-03-01

DOI

10.1007/s00271-013-0417-x

Peer reviewed

eScholarship.org Powered by the California Digital Library
University of California

Irrig Sci (2014) 32:111–125
DOI 10.1007/s00271-013-0417-x

ORIGINAL PAPER

HYDRUS simulations of the effects of dual-drip subsurface irrigation and a physical barrier on water movement and solute transport in soils

Mohammad N. El-Nesr · A. A. Alazba · Jiří Šimůnek

Received: 9 March 2013 / Accepted: 16 September 2013 / Published online: 4 October 2013
© Springer-Verlag Berlin Heidelberg 2013

Abstract Subsurface drip irrigation systems, compared to other irrigation systems, enhance the delivery of water and nutrients directly into the root zone. However, in light-textured soils, certain quantities of water may percolate below the root zone due to the subsurface position of drip lines and/or poor management of irrigation systems. The main objective of this paper is to evaluate three technologies to enhance a spatial distribution of water and solutes in the root zone and to limit downward leaching. The three technologies include (a) a physical barrier, (b) a dual-drip system with concurrent irrigation, and (c) a dual-drip system with sequential irrigation. To achieve this objective, we performed computer simulations using the HYDRUS (2D/3D) software for both bare and vegetated soils. The results indicate that the physical barrier is more efficient than dual-drip systems in enhancing the water distribution in the root zone while preventing downward leaching. On the other hand, the dual-drip system improves water distribution in sandy soils. Additionally, the dual-drip system with sequential irrigation, followed by the dual-drip system with concurrent irrigation, is the most efficient in limiting downward leaching of solutes.

Communicated by N. Lazarovitch.

M. N. El-Nesr (✉) · A. A. Alazba
Alamoudi Chair for Water Research, King Saud University, Riyadh, Saudi Arabia
e-mail: drnesr@gmail.com; melnesr@ksu.edu.sa

J. Šimůnek
Department of Environmental Sciences, University of California Riverside, Riverside, CA, USA

Introduction

Surface and subsurface drip irrigation (SDI) systems are increasingly being used in arid regions with limited water resources to irrigate agricultural crops. The SDI systems have an especially promising future due to their many advantages. The main advantages of SDI, compared to surface drip irrigation (DI), include the following: (a) a significant reduction in evaporation, (b) a direct application of water and fertilizers into the root zone (Phene et al. 1987; Reich et al. 2009), and (c) an easier and, for drip lines, safer operation of machinery.

The proper design of SDI systems requires knowledge of the water distribution patterns around the emitters that match the root extraction patterns and minimize wetting of the soil surface and deep percolation (Kandelous et al. 2011). The exact shape of the wetted volume and water distribution depends on many factors, including soil hydraulic characteristics, initial soil conditions, discharge rate, application frequency, root characteristics, evaporation, and transpiration (Subbaiah 2013). Additionally, the wetting pattern depends on the location of the emitter with respect to the soil surface. For uniform and homogeneous soils, the theoretical wetting pattern is hemiellipsoidal or ellipsoidal when the dripper is located on the soil surface or in the subsurface, respectively.

Generally, plants have higher root densities in the upper part of the root zone. It was reported that in a surface-irrigated soil profile with a uniform water content, most plants extract about 40, 30, 20, and 10 % of their water needs from corresponding quarters of the root zone (Hansen et al. 1980; Ayers and Westcot 1985; Majumdar 2004). However, the root extraction pattern from a subsurface-irrigated soil profile may be different. Despite a similar wetting pattern under DI and SDI systems, a considerable

amount of water escapes from the root zone by percolating downward or dispersing laterally in the soil beyond the reach of roots. El-Berry (1989) reported that the main avenue for water losses under SDI is deep percolation, which is highest during the seedling stage and declines with the growth of the root system.

Several investigators have tried to adjust the shape of the wetted zone to better match the root extraction pattern (e.g., Phene et al. 1987; Barth 1995; Welsh et al. 1995; Elawady et al. 2003; Ismail et al. 2006). Phene et al. (1987) showed that the wetted pattern around the buried emitter can be managed by adjusting the irrigation frequency and that more water moves toward the soil surface when the irrigation frequency is increased. Other investigators (e.g., Barth 1995; Welsh et al. 1995; Brown et al. 1996) have suggested placing an impermeable barrier below the lateral drip lines. This barrier can be made of polyethylene (Barth 1995; Brown et al. 1996) or metal (Welsh et al. 1995). It has been reported by several investigators that the physical barrier leads to a significant increase in crop yield in sandy soils. For example, an increase in spinach yield by 18 % was reported by Elawady et al. (2003) and in tomato yield by 141–190 % by Awady et al. (2008). ElNesr (2011) reported for a Sinai sandy dunes soil an increase in tomato yield by 119 % and in Jerusalem artichoke yield by 131 %. These large increases in crop yield due to the presence of a physical barrier were attributed to the high infiltration rate of the sandy soil (e.g., 67 cm/h in the experiments of ElNesr (2011)), with the physical barrier preventing downward water percolation and keeping water in the root zone. On the other hand, there are several problems concerning this physical barrier. For example, there are technical and economic problems with digging a wide and deep trench to install the physical barrier. There may also be physiological problems for the root system, related to root rot and/or shallow root disease. Additionally, there are potential hazards of salt accumulation and other toxicity problems related to accumulation of fertilizers and other chemicals. Hence, the physical barrier should not be used except in soils with very high infiltration rates.

Several investigators have attempted to achieve similar goals using capillary barriers, i.e., improved water content distributions (Kampf et al. 1998 and Morris and Stormont 1998) and increased crop yields (Ityel et al. 2010, 2011). A capillary barrier is an interface between two soil layers having distinct differences in hydraulic characteristics, such as a fine soil layer overlaying a coarse-textured soil (Kampf et al. 1998). Ityel et al. (2010) found that the presence of a capillary barrier increased volumetric soil water contents by 20–70 %, depending on the soil texture and a depth of a barrier, and corresponding yields of pepper and lettuce by 25 and 36 %, respectively, while having a negligible effect on the yields of tomatoes and melons (Ityel et al. 2011).

Ismail et al. (2006) attempted to modify the wetting pattern by burying a secondary drip line beneath the primary one and by dividing the required water volume between the two drip lines. They hypothesized that water moves faster into the dry soil (due to the higher pressure head gradient) than into the moist soil, and thus, when the secondary drip line moistens the soil below the primary drip line, it forces water from the upper drip line to redistribute upward and laterally, rather than moving downward. Hence, they called this technique "a hydraulic barrier". This technique requires no wider trenching than the normal SDI trenching and prevents all the above-discussed risks to roots. Note that water applications may be adjusted between the upper and lower emitters depending on root depth and root density, and more water may be applied through the upper emitter during the early growth stages when the plant roots are shallow. Ismail et al. (2006) reported two complimentary irrigations during the first 2 weeks of the plant growth. Their results showed that when applied in the field, the hydraulic barrier increased the total and marketable yields of the Jerusalem artichokes by 12 and 48 %, respectively. These results clearly document the benefits of using such techniques to increase crop yields under specific circumstances.

In order to efficiently design and manage SDI systems, several models (analytical and empirical) have been developed to describe water flow from an emitting source (a point or line source) in the soil (surface or subsurface) (e.g., Brandt et al. 1971; Warrick 1985; Revol et al. 1997; Khalifa et al. 2004; Singh et al. 2006). One of the most complete packages for simulating water, heat, and solute movement in both two- and three-dimensional, variably saturated, porous media is the HYDRUS software package (Šimůnek et al. 2008). Many investigators have used this model to evaluate either field or laboratory experiments, or other mathematical models (e.g., Skaggs et al. 2004; Lazarovitch et al. 2005; Provenzano 2007; Zhou et al. 2007; Kandelous and Šimůnek 2010a, b; Ramos et al. 2012). The HYDRUS model enables its users to trace the movement of water and solutes and the wetting patterns in both simple and complex geometries for homogeneous or heterogeneous soils and for different combinations of initial and boundary conditions (BCs).

The main objectives of this study therefore are (a) to simulate water flow and solute transport for an SDI system while considering both the physical barrier and the dual-drip system using the HYDRUS package and (b) to numerically evaluate how these techniques affect the movement of water and solutes in the soil and whether or not the dual-drip system can act as a hydraulic barrier for movement of water and solutes.

Materials and methods

SDI modeling

Soil water and solute distributions around a buried drip source were simulated using the numerical model HYDRUS (2D/3D) (Šimůnek et al. 2011). The model simultaneously solves numerically the Richards equation and the advection–dispersion equation for variably saturated water flow and solute transport in soils, respectively. The Richards equation governing water flow from a point source through variably saturated, porous media can be written in axisymmetric coordinates as follows:

$$\frac{\partial\theta}{\partial t}=\frac{1}{r}\frac{\partial}{\partial r}\left[rK(h)\frac{\partial h}{\partial r}\right]+\frac{\partial}{\partial z}\left[K(h)\frac{\partial h}{\partial z}\right]-\frac{\partial K(h)}{\partial z}-S(h) \tag{1}$$

where θ is the volumetric water content [L^3L^{-3}], t is the time [T], h is the soil water pressure head [L], r is the radial (horizontal) coordinate [L], z is the vertical coordinate that is positive upward [L], $K(h)$ is the unsaturated hydraulic conductivity [LT^{-1}], and $S(h)$ is the sink term representing root water uptake expressed as a volume of water removed from a unit volume of soil per unit time [$L^3L^{-3}T^{-1}$].

The soil water retention was modeled using the van Genuchten equation (van Genuchten 1980),

$$S_e=\frac{\theta-\theta_r}{\theta_s-\theta_r}=\frac{1}{(1+(\alpha h)^n)^m} \tag{2}$$

where S_e is the effective degree of saturation or the reduced water content [–], θ_r and θ_s are the residual and saturated water contents [L^3L^{-3}], respectively, α is an empirical parameter [L^{-1}] inversely related to the air entry value, and n and m are empirical constants affecting the shape of the retention curve [–]. The value of m is restricted by $m = 1 - 1/n$.

The hydraulic conductivity as a function of S_e was assumed to be described using the closed form equation of van Genuchten (1980), which combines the analytical expression (2) with the pore size distribution model of Mualem (1976):

$$K(S_e)=K_sS_e^{\Upsilon}\left(1-\left(1-S_e^{\frac{1}{m}}\right)^m\right)^2 \tag{3}$$

where Υ is the pore connectivity parameter estimated by Mualem (1976) to be about 0.5 as an average for many soils and K_s is the saturated hydraulic conductivity [LT^{-1}].

The sink term $S(h)$ was computed using the Feddes et al. (1978) model adapted for a radially symmetric problem:

$$S(h)=\alpha(h)S_p=\alpha(h)\beta(r,z)A_TT_p \tag{4}$$

where S and S_p are the actual and potential (during no-stress periods) root water uptake rates [$L^3L^{-3}T^{-1}$], respectively, $\alpha(h)$ is a dimensionless water stress response function for water uptake by plant roots (Feddes et al. 1978), $\beta(r, z)$ is a function describing the spatial root distribution (Vrugt et al. 2001) [L^{-3}], T_p is the potential transpiration rate, and A_T is the surface area associated with transpiration [L^2].

The advection–dispersion equation governing the transport of a single non-reactive ion in a homogeneous, radially symmetric, porous medium can be described as:

$$\frac{\partial\theta c}{\partial t}=\frac{1}{r}\frac{\partial}{\partial r}\left(r\theta D\frac{\partial c}{\partial r}\right)+\frac{\partial}{\partial z}\left(\theta D\frac{\partial c}{\partial z}\right)-\frac{\partial(q_rc)}{\partial r}-\frac{\partial(q_zc)}{\partial z} \tag{5}$$

where c is the concentration in the liquid phase [ML^{-3}], D is the effective dispersion coefficient [L^2T^{-1}], and q_r and q_z are the volumetric flux densities in r and z directions, respectively, [LT^{-1}].

Modeled scenarios

To address our main objectives, we have chosen to evaluate the following alternative scenarios:

1. Two soil textures (sand and loam).
2. Bare or vegetated soil profiles.
3. Different water applications:
   - 3.1 A single emitter without a physical barrier (denoted below as case a)
   - 3.2 Two emitters operating concurrently (case b).
   - 3.3 Two emitters operating sequentially (the upper emitter starts operating 30 min before the lower one) (case c).
   - 3.4 A single emitter with a physical barrier (case d).
4. Different solute applications:
   - 4.1 Water and solute are applied from a single emitter without a physical barrier (case a).
   - 4.2 Water is applied from both emitters, and solute is applied only from the upper emitter. The upper emitter starts operating 30 min before the lower one (case c).
   - 4.3 Same as 4.2, but the upper emitter starts operating 120 min before the lower one (case c_u).
   - 4.4 Same as 4.2, but the upper emitter starts operating 120 min after the lower one (case c_d).
   - 4.5 Water and solute are applied from a single emitter in the presence of a physical barrier (case d).

Note that the term "case" refers to the operation sequence (i.e., one emitter with or without a physical barrier and two emitters operating either concurrently or sequentially). The same "case" indicates simulations with

Table 1 Physical properties of soils considered in HYDRUS simulations

Soil texture	Bulk density (g cm^{-3})	Residual soil water content (cm^3 cm^{-3})	Saturated soil water content (cm^3 cm^{-3})	Parameter α in the soil water retention function (cm^{-1})	Parameter n in the soil water retention function (−)	Saturated hydraulic conductivity, K_s (cm min^{-1})	Tortuosity parameter Υ in the conductivity function (−)
Sand	1.64	0.045	0.43	0.145	2.68	0.49500	0.5
Loam	1.50	0.078	0.43	0.036	1.56	0.01733	0.5

Table 2 Root water uptake parameters for analyzed crops

Crop	Values of the pressure head (cm) below which root water extraction …					Limiting potential transpiration rates (cm/min)	
	…starts. (h_1)	…occur at the maximum possible rate (h_2)	…starts to decline from the maximum rate at the potential transpiration rate equals…		…stops (h_4)		
			… R_2^{High} (h_3^{High})	… R_2^{Low} (h_3^{Low})		Highest (R_2^{High})	Lowest (R_2^{Low})
Tomatoes	−10	−25	−500	−600	−1,000	0.008007	6.944e−5
Potatoes	−10	−25	−300	−500	−800	0.00766	6.944e−5

Table 3 Parameters describing a spatial root distribution for analyzed crops

Parameters	Potatoes	Tomatoes
Maximum rooting depth (cm)*	50	40
Depth of maximum root uptake intensity (cm)	10	15
Maximum rooting radius (cm)	80	60
Radius of maximum root uptake intensity (cm)	15	15
Surface area associated with transpiration, A_T (cm^2)	4,000	10,000

* When no physical barrier is considered

or without solute. The timing of emitters operating sequentially is indicated by subscripts u and d for case c.

Properties of soils, crops, and solutes considered in HYDRUS simulations

Simulations were carried out for soils representing two textural classes: sand and loam. Soil hydraulic parameters for the two textural classes were taken from the soil catalog provided by the HYDRUS software (Carsel and Parrish 1988) and are given in Table 1.

Parameters representing two model crops, tomatoes (*Solanum lycopersicum*) and potatoes (*Solanum tuberosum*), were used in the simulations. The stress response function of the root water uptake model for selected crops was defined according to Feddes et al. (1978), and its parameters are listed in Table 2. Parameters describing the spatial root distribution according to the model of Vrugt et al. (2001) were taken from ElNesr et al. (2012) and are listed in Table 3. These parameters were considered constant with time, since the current version of HYDRUS does not support a time-variable spatial root distribution. Also, the same root spatial distribution was considered for both soil types. Although in reality, the root spatial distribution varies dynamically with the soil water content, the age of the plant, the soil type, and the emitter's location (Coelho and Or 1999), since the duration of our simulations (either one irrigation cycle for water flow or 30 days for solute transport scenarios) was relatively short, an assumption of a constant root spatial distribution seemed adequate.

A non-reactive solute tracer was considered in solute transport simulations. The soil profile was considered to be initially solute free (zero concentration), and a unit concentration was applied during solute applications through the main (upper) emitter. The longitudinal and transverse dispersivities were considered with values of 5 and 0.5 cm, respectively, while the molecular diffusion was neglected (Radcliffe and Šimůnek 2010). Since our interest was mainly in the transport pathways and leaching of the studied solute, the root solute uptake was neglected as well. Cauchy and Neuman BCs were considered at the emitter and outflow boundaries, respectively.

Transport domain, initial and boundary conditions

The HYDRUS (2D/3D) software package (version 2.02) (Šimůnek et al. 2008) is used in numerical simulations for all modeled scenarios. Water flow, root water uptake, and solute transport are the processes considered in the simulations. The transport domain for all scenarios was considered to be axisymmetrical around a vertical axis,

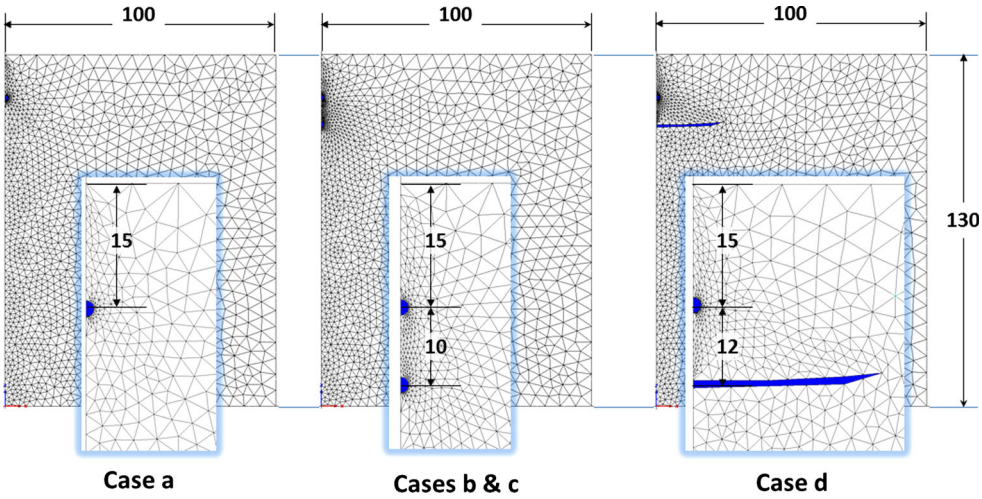

Fig. 1 Location of the emitters and the physical barrier in the transport domain (discretized using unstructured finite element mesh) considered in HYDRUS simulations: a domain around a dripper is magnified in excerpts. Dimensions are given in cm

Fig. 2 The transport domain with applied boundary conditions

similarly as done by many other researchers (e.g., Gärdenäs et al. 2005; Lazarovitch et al. 2005; Kandelous et al. 2011). Figure 1 shows the detail of the upper left corner of the transport domain, in which the emitters and a physical barrier are located. The transport domain was 100 cm wide (radius) and 130 cm deep (depth), i.e., large enough so that an overlap in water content profiles from neighboring emitters (on other laterals) do not have to be considered. The (upper) emitter was located 15 cm below the soil surface (Fig. 1, left), while the secondary emitter (in scenarios b and c) was 25 cm below the soil surface (Fig. 1, center). The physical barrier (when considered, scenario d) was placed 27 cm below the soil surface and was considered to have a radius of 25 cm (Fig. 1, right). The soil profile was considered to be homogeneous (with different soil types considered in different simulations) and initially uniformly dry, with the initial pressure head of −1,000 cm. In the scenarios with solute transport, the soil profile was considered to be initially solute free (zero concentration). Soil evaporation from bare soil was neglected.

Figure 2 shows the BCs considered in different scenarios in this study. In all simulated scenarios, the upper boundary of the transport domain was subjected to atmospheric conditions, while the lower boundary of the domain was free drainage. Boundaries at both vertical sides were assigned a "no-flux" BC. Emitters were represented in all cases as half circles with a radius of 1 cm, located on the left vertical boundary of the transport domain. The upper emitter was assigned a "Variable Flux 1" BC. In scenarios b and c, in which two emitters were considered, the second emitter was assigned a "Variable Flux 2" BC. In scenario d, the physical barrier was simulated as a 1-cm-thick impermeable barrier 25 cm wide with a "no-flux" BC (Figs. 1d, 2). The transpiration rate was considered to be constant with time and equal to 4.0 mm/day, i.e., daily variations of the transpiration rate were not considered.

Since it is common to irrigate vegetables every 2–3 days (e.g., Allen et al. 1998), simulations were carried out for 2,880 min (i.e., 2 days) when only water flow was considered. When solute transport was also simulated, the same irrigation conditions (the main cycle) were repeated 15 times, resulting in the total time of 30 days.

Time-variable BCs were used to simulate DI. Since vegetables are widely irrigated using 1-gph (gallon per hour; 3.7 L/h) pressure-compensating emitters (especially in Saudi Arabia where this research was carried out), this discharge was used for the dual-drip system ($3.7 \times 2 \cong 7.5$ L/h). The total discharge (Q) was considered to be 7.5 L/h, which is equivalent to a steady-state flux

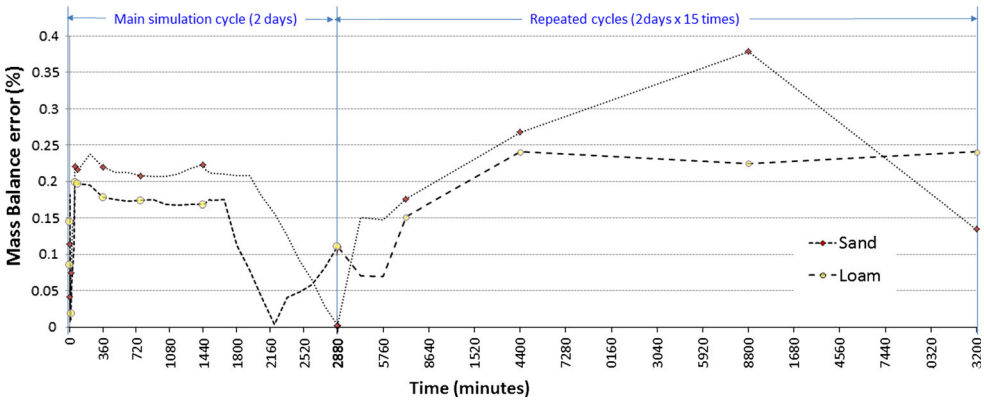

Fig. 3 Water mass balance error in a 30-day simulation scenario (case d, bare sand and loam soils)

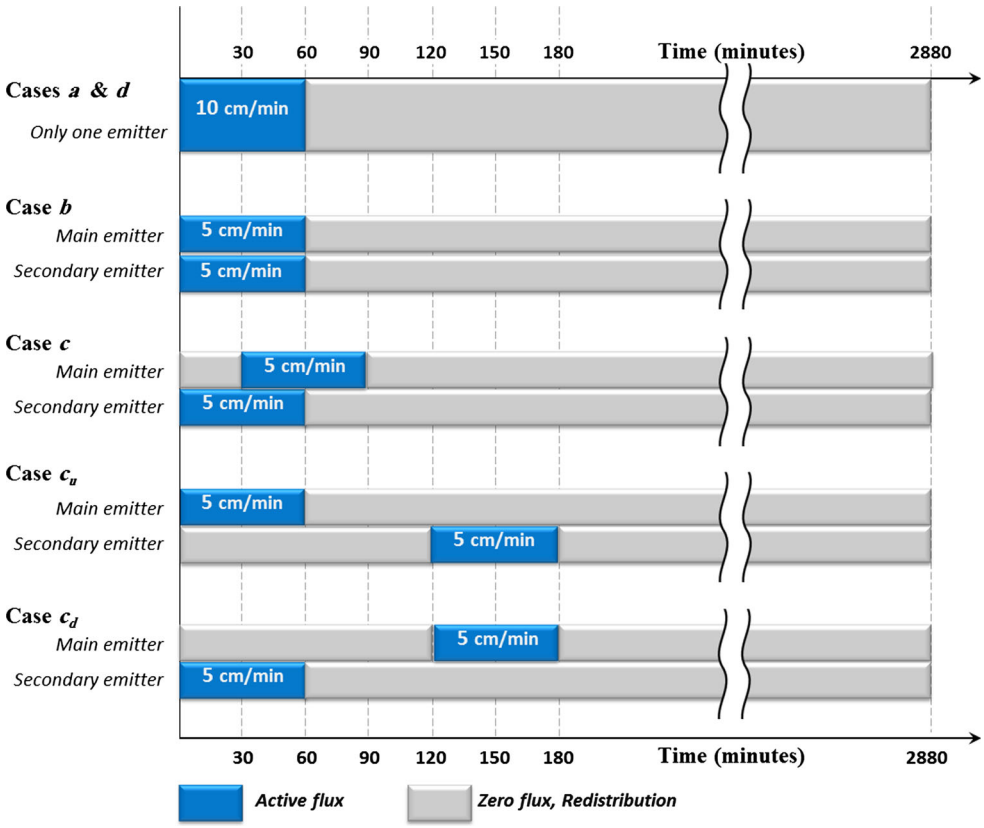

Fig. 4 Irrigation fluxes applied in different scenarios

of about 10 cm/min [$q = Q/4\pi r^2$, where q is the boundary flux (cm/min), Q is the emitter discharge (cm^3/min), and r is the wetted radius of the emitter (cm)]. In scenarios with a single emitter (cases a and d), the irrigation flux was 10 cm/min. In scenarios with two emitters (cases b and c), the irrigation flux at each emitter was 5 cm/min, thus maintaining the same total discharge in all scenarios. Since this discharge flux is significantly larger than the saturated hydraulic conductivity of the two selected soils, the positive pressure heads developed at boundaries representing the emitters. Although HYDRUS has an option to reduce the emitter discharge depending on this back pressure (Lazarovitch et al. 2005), in order to avoid the need for additional parameters and since we assume the emitters to be pressure compensating, a constant discharge was considered also during this time period, allowing a buildup of positive pressures at the emitters. The numerical mass balance was continuously checked in all simulations, with a target not to exceed the mass balance error of 1.0 %. The largest recorded mass balance error in all simulations was 0.68 %. An example of the development of the mass balance error in one 30-day simulation is presented in Fig. 3.

The operation sequence of different emitters in different scenarios is shown in Fig. 4. In cases a and d with only one emitter, this emitter operates for 60 min every 2 days. In case b with two emitters, the two emitters have the same

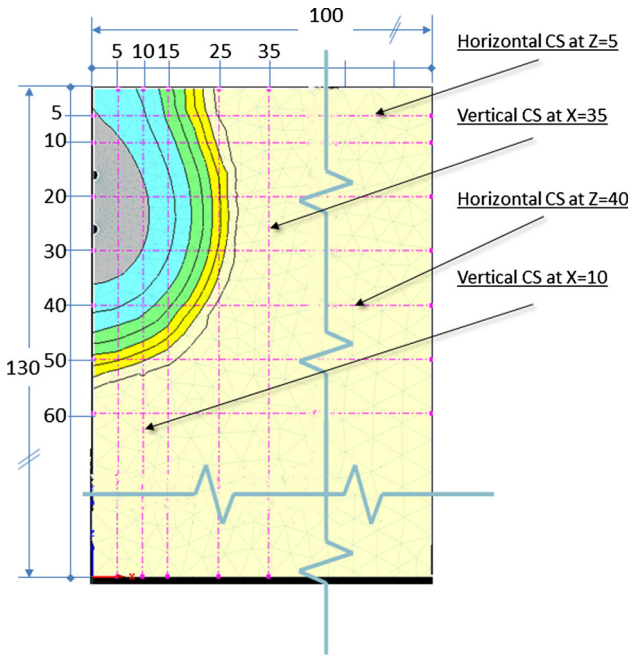

Fig. 5 Locations of analyzed cross sections (CS) in the transport domain

duration of operation, but with only 50 % flux applied to each of them. Finally, for cases c, c_u, and c_d with two emitters operating sequentially, Fig. 4 shows the pattern of each sequential operation. The secondary (deeper) emitter starts operating either 30 or 120 min before the main (upper) emitter in cases c and c_d, respectively, or 120 min after the upper emitter in case c_u. Again, in these sequential scenarios, the irrigation flux to each emitter is half of the flux in cases a and d.

In the "Results and discussion" section below, we will provide graphical outputs for pressure heads along vertical and horizontal cross sections throughout the transport domain. Five vertical cross sections are at radial distances of 5, 10, 15, 25, and 35 cm away from the axis of symmetry, while seven horizontal cross sections were defined at depths of 5, 10, 20, 30, 40, 50, and 60 cm. The transport domain and the analyzed cross sections are illustrated in Fig. 5.

Results and discussion

Simulation results for water flow

In this section, we will discuss the results of numerical simulations for different cases and for two soils. For each soil, we will discuss both water content profiles along horizontal and vertical cross sections for nine output times with an increasing time interval, i.e., 1, 5, 20, 60, 90, 360, 720, 1,440, and 2,880 min after the beginning of infiltration. Displayed water content profiles thus cover both the infiltration and redistribution parts of the numerical experiment. We will discuss first the results for bare soils and then for vegetated soils. Since we did not observe any significant differences between results obtained for two considered crops, only those obtained for tomatoes will be presented and discussed below.

Bare, loamy soil

Water distribution along vertical cross sections Figure 6 shows the vertical water content distributions at five vertical cross sections at distances of 5, 10, 15, 25, and 35 cm from the emitter(s) for the bare, loamy soil for four analyzed scenarios (a–d). Multiple curves represent outputs at different times.

The irrigation scheme can be clearly identified from the water content profiles after 1 min in the 5 cm from the emitter cross section (Fig. 6, left). While water content profiles for cases a and d clearly show infiltration from a single emitter, for case b, they show infiltration from two emitters, and for case c only from the bottom emitter, since the upper emitter starts operating only after 30 min. In case a, the area around the emitter (depths of 8–25 cm) at a distance of 5 cm reached saturation before 5 min. This area (at a 5 cm distance from the emitter) continues to widen until about 30 cm of the soil profile around the emitter is saturated at the end of irrigation. The water content profile after 60 min already reflects the redistribution process, since the irrigation flux stops at 60 min in all cases except c (as shown in Fig. 4). The root zone is close to full saturation for the longest period of time for case c (in which case, irrigation from the upper dripper stops at 90 min), followed by case d.

Water content profiles are quite similar at a 10 cm distance from the emitter, except in case d, which shows some noticeable differences in the upper 25 cm. Maximum water contents are reached in case c at times of 60 and 90 min. At a 15 cm distance from the emitter, the highest water contents are reached in case d in the upper 25 cm, while the three other cases are quite similar. At a 25 cm distance, only small increases in water contents can be observed over time. While the first increase in the water content is observed only after 60 min in cases b and c, this occurs earlier (after 20 min) in cases a and d due to the higher irrigation flux from a single emitter.

Interestingly, at a 25 cm distance, water content values appear in reverse order versus time compared to water content values at shorter distances. While at this distance water contents are increasing for larger times, at shorter distances they are decreasing. This is due to the redistribution process, which drives water both vertically and

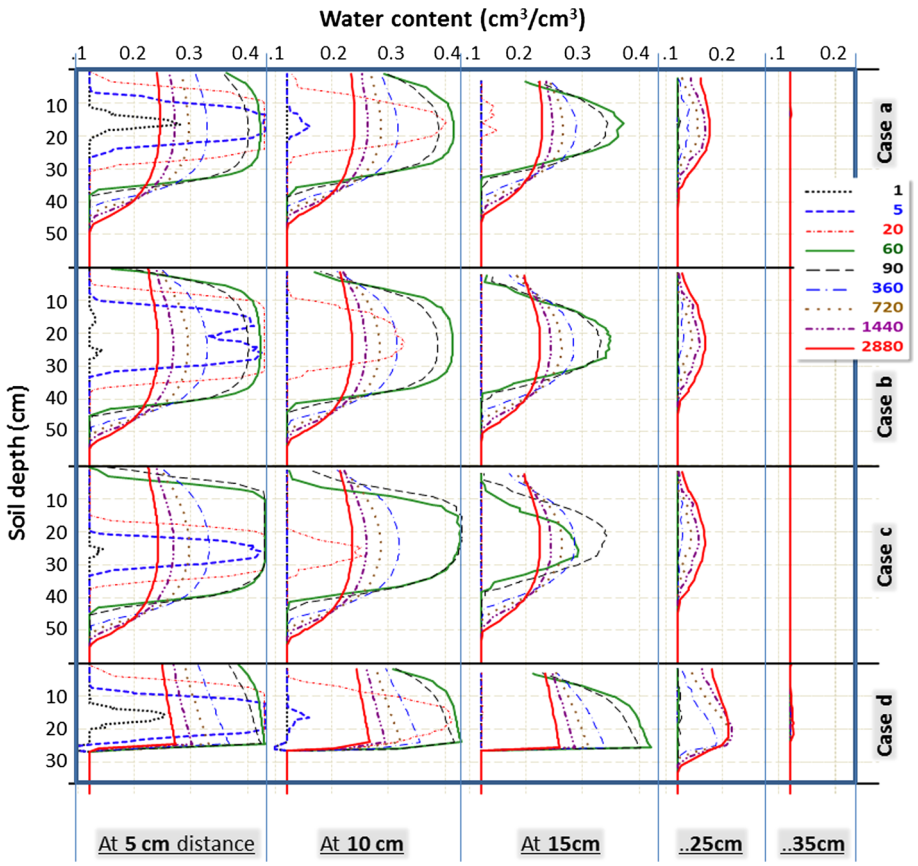

Fig. 6 Vertical water content distributions at different distances (5, 10, 15, 25, and 35) away from the dripper for different irrigation scenarios for a bare, loamy soil

laterally to distances further from emitters. Finally, notice that water did not reach the 35 cm distance, except in case d between depths of 10 and 25 cm.

Water distribution along horizontal cross sections Water content distributions for four analyzed cases are shown in Fig. 7 at seven horizontal cross sections at depths of 5, 10, 20, 30, 40, 50, and 60 cm. The same output times as in Fig. 6 are shown. In cases b and c, the highest water contents are found at a depth of 20 cm, i.e., between the main and secondary emitters, which are placed at depths of 15 and 25 cm, respectively. In this depth, the soil stays saturated to a horizontal distance of about 20 cm for up to about 90 min in case c. In case d, water contents are highest compared to other scenarios at all times at depths of 5, 10, and 20 cm, while only a small amount of new water appears at a 30-cm depth at the far end of the physical barrier at later times (at about 360 min). This is due to the redistribution process, which is demonstrated in Fig. 8. Figure 8 shows that the physical barrier is very effective in preventing the leaching of water to deeper depths, as only small quantity of water flows around the barrier.

While water content profiles for the first three cases a, b, and c are quite similar in the top 30 cm (Fig. 7), substantial differences occur at a depth of 40 cm and below. While in case a, at a depth of 40 cm, the maximum water content is only about 0.2 cm^3 cm^{-3}, in both cases b and c, water contents are as much as 0.38 at 90 min and 0.3 at 360 min. Only cases b and c show increases in water contents (up to 0.20) at later times due to the redistribution process (at times of 720, 1,440, 2,880 min). None of the analyzed cases delivered water down to a 60-cm depth.

Bare, sandy soil

Water distribution along vertical cross sections Sandy soils have significantly higher hydraulic conductivities and infiltration rates than loamy soils and significantly lower macroscopic capillary length (e.g., Radcliffe and Šimůnek 2010). This causes water to move deeper and much less laterally into the sandy soil profile than in the loamy soil. Our simulations very clearly show this in Fig. 9. In cases b and c, water infiltrated down to 60 and 90 cm at a 5 cm distance at times 60 and 2,880 min, respectively. On the other hand, the rest of the profile is much less saturated. Although water contents around emitters are higher than 0.40, water quickly redistributes when irrigation stops. The highest water contents around the emitter at all times can be observed in case d because of the physical barrier, which prevents redistribution of water downward, while physical properties of the sandy soil prevent lateral

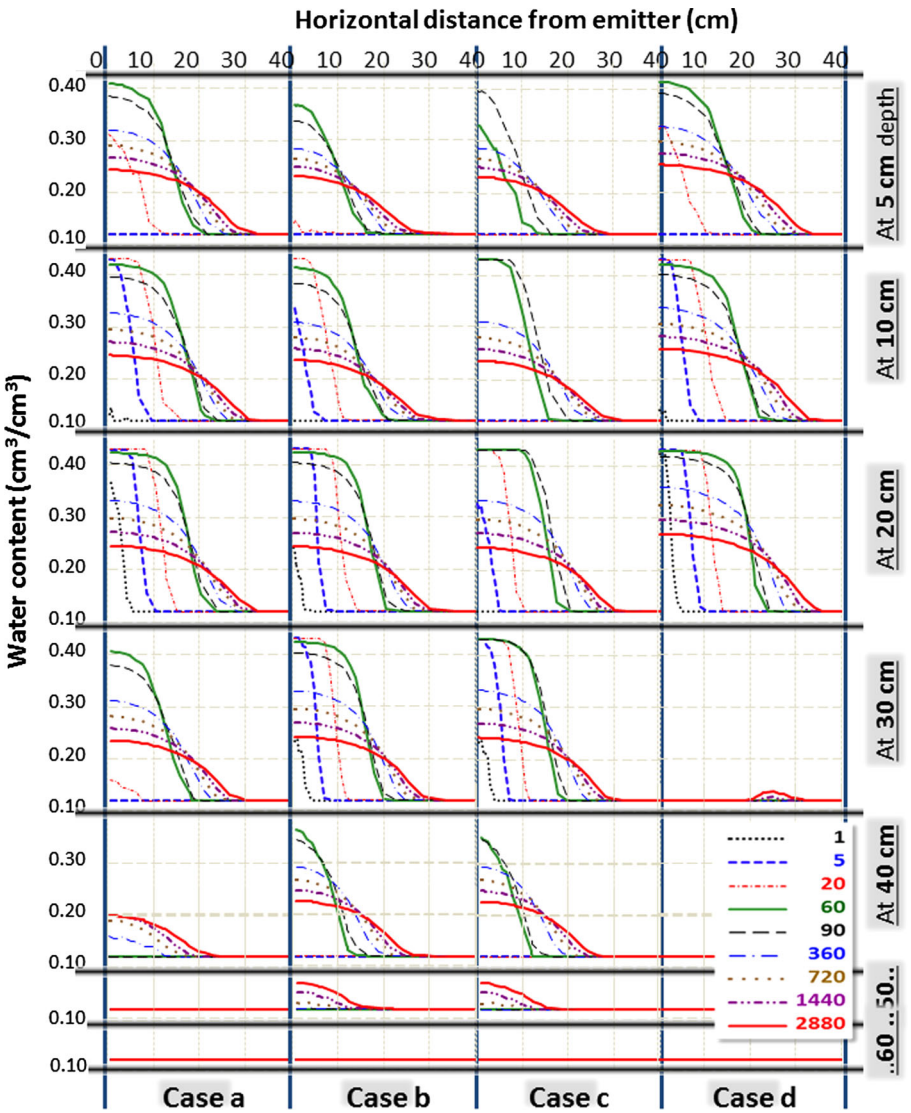

Fig. 7 Horizontal water content distributions at different depths (5, 10, 20, 30, 40, 50, and 60) for different irrigation scenarios for a bare, loamy soil

redistribution. In case c, the highest water contents are reached at 90 min when irrigation from the primary emitter stops.

There are only very small differences in water content profiles between the first three cases after 360 min. This shows that none of the analyzed cases, except case d, improve the wetting pattern once redistribution in the sandy soil starts. The same phenomena can be observed at cross sections at a distance of 10 and 15 cm. On the other hand, in case d, one can observe the accumulation of water above the physical barrier, as well as its bypassing during the redistribution process (at the 25- and 35-cm cross sections). This shows that the physical barrier indeed enhances water redistribution in the root zone.

Water distribution along horizontal cross sections One of the main benefits of the SDI is that it keeps a dry soil surface. This helps to reduce the loss of water due to evaporation and prohibits the growth of weeds at the soil surface. Cases b and c have the lowest water contents in the top 5 cm of the soil profile (Fig. 10). This is caused mainly by the lower value of the discharge (5 cm/min) of the upper emitter in the case of the dual-drip system compared to the single-drip system (10 cm/min). This may be considered one of the benefits of the dual-drip system.

At a 10-cm depth, the highest water contents for cases a and d occur at 20 min, while for case c, the highest water contents occur at times of 60 and 90 min. No noticeable differences are visible between cases a–c from time 360–2,880 min. In case d, water laterally spreads both above (at higher values) and below the physical barrier, moving more than 40 cm at times of 1,440 and 2,880 min, while in other cases, the lateral spreading is at most 30 cm. At a 20-cm depth, the highest water contents were obtained in case d at almost all times. This reflects the role of the physical barrier. Case c has the second highest water

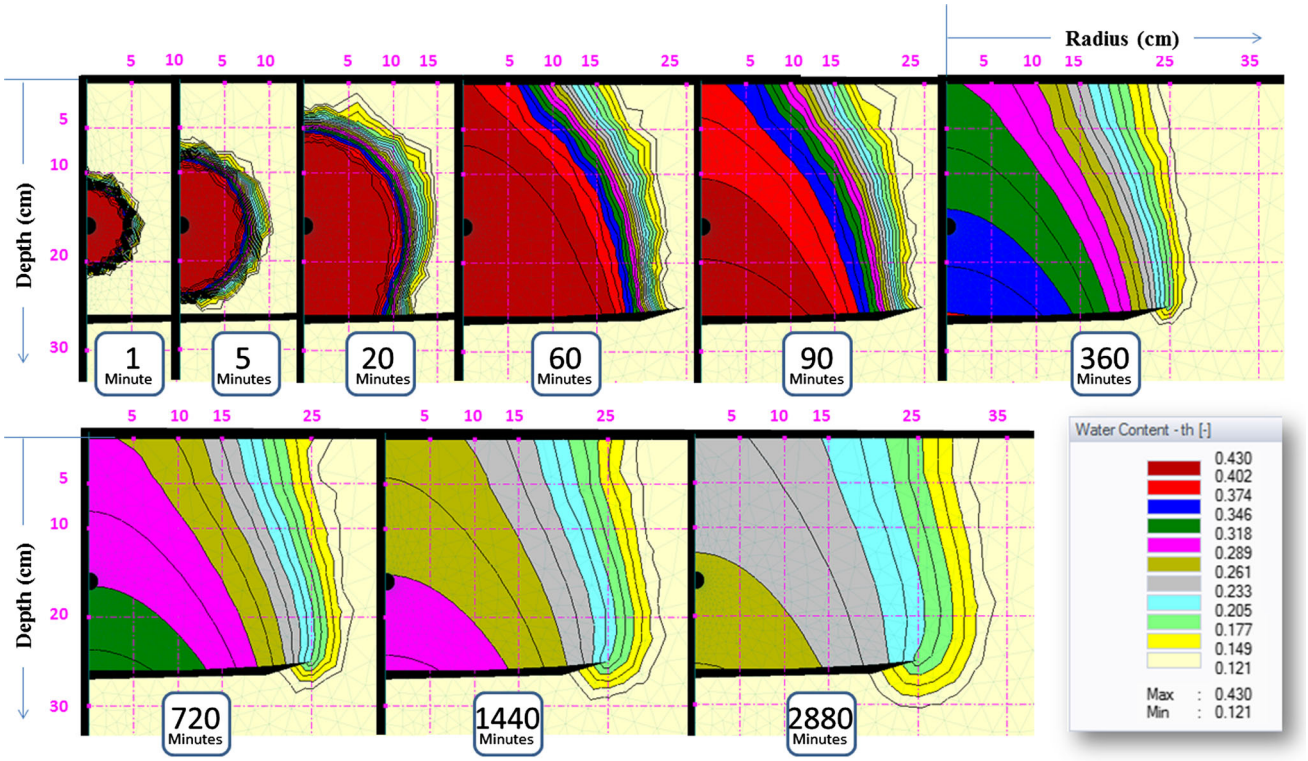

Fig. 8 Water content distributions at different times for case d for a bare, loamy soil

Fig. 9 Vertical water content distributions at different distances (5, 10, 15, 25, and 35) away from the dripper for different irrigation scenarios for a bare, sandy soil

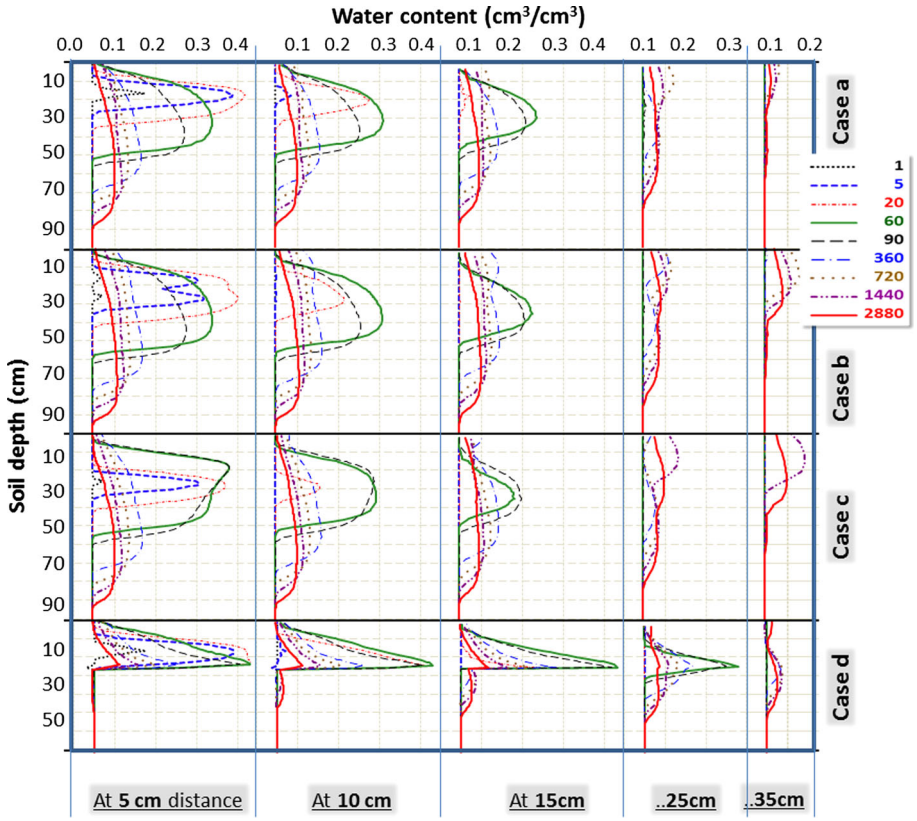

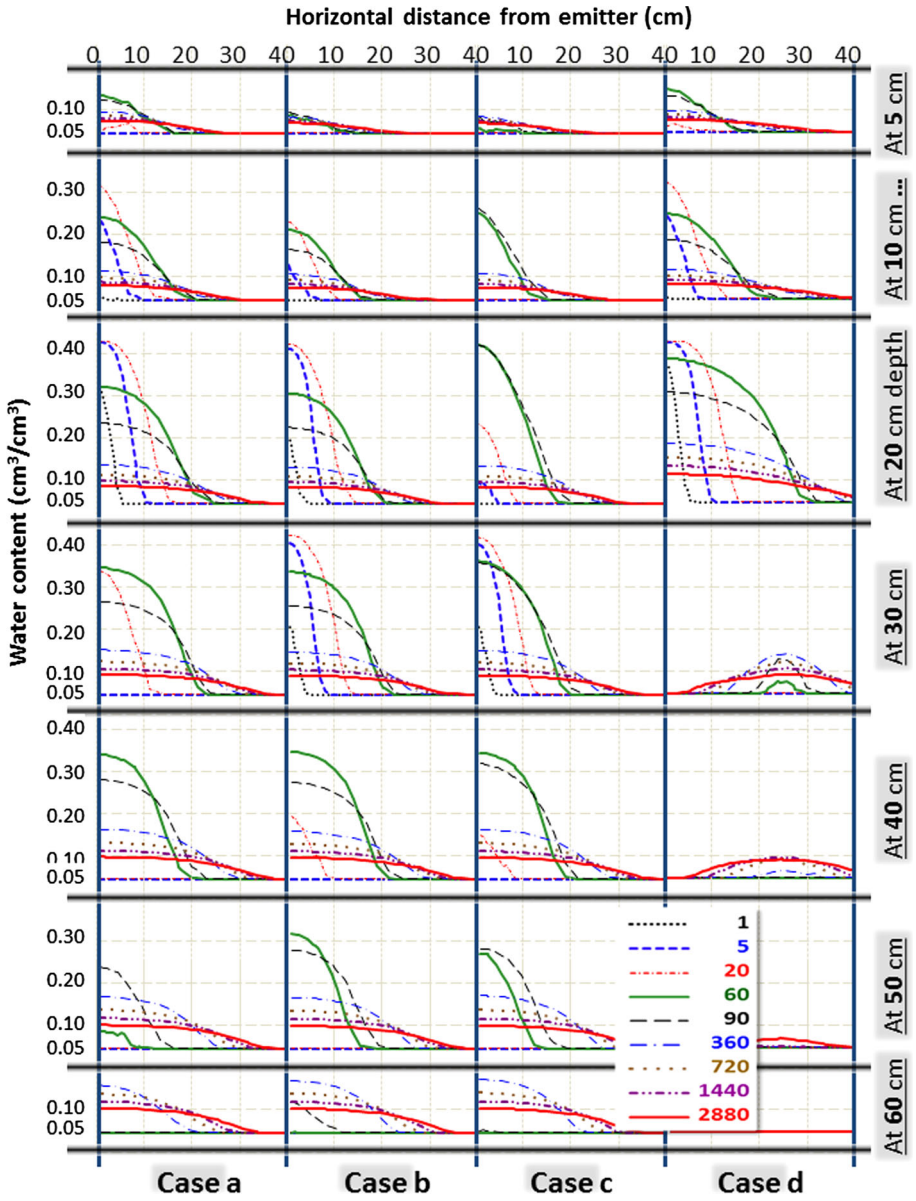

Fig. 10 Horizontal water content distributions at different depths (5, 10, 20, 30, 40, 50, and 60 cm) for different irrigation scenarios for a bare, sandy soil

content with a near-saturation state for up to 90 min. This reflects the effect of the sequential operation of the dual-drip system. At depths of 30 and 40 cm, the highest water contents were obtained in case c at 90 min, while the lowest water contents were obtained in case d due to the existence of the physical barrier at a depth of 27 cm. In case d, there was almost no water content increase at a depth of 50 cm and no increase at all at a depth of 60 cm. On the other hand, the dual-drip scenarios (cases b and c) show a better distribution of water at a depth of 50 cm than case a up to 90 min.

Bare soil comparisons In the loamy soil, water never reached, except in case d, the radial cross section of 35 cm (Fig. 6). Additionally, in none of the analyzed cases water moved down to a depth of 60 cm (Fig. 7). On the other hand, for the sandy soil, Fig. 9 clearly shows that water reached (although in only small amounts) the radial distance of 35 cm at times 1,440 and 2,880 in all cases, and especially in cases b and c. Moreover, water also moved downward and reached depths of 60 and 90 cm (Fig. 10). Therefore, the commonly observed fact that water moves deeper and much less laterally in the sandy soil than in the loamy soil is not exactly true for the conditions studied. In the sandy soil, in addition to moving deeper in the soil profile than in the loamy soil, water also moved more laterally when the dual-drip subsurface system was used. These findings show the advantage of the dual-drip subsurface systems, i.e., these systems improve the redistribution of water applied in sandy soils.

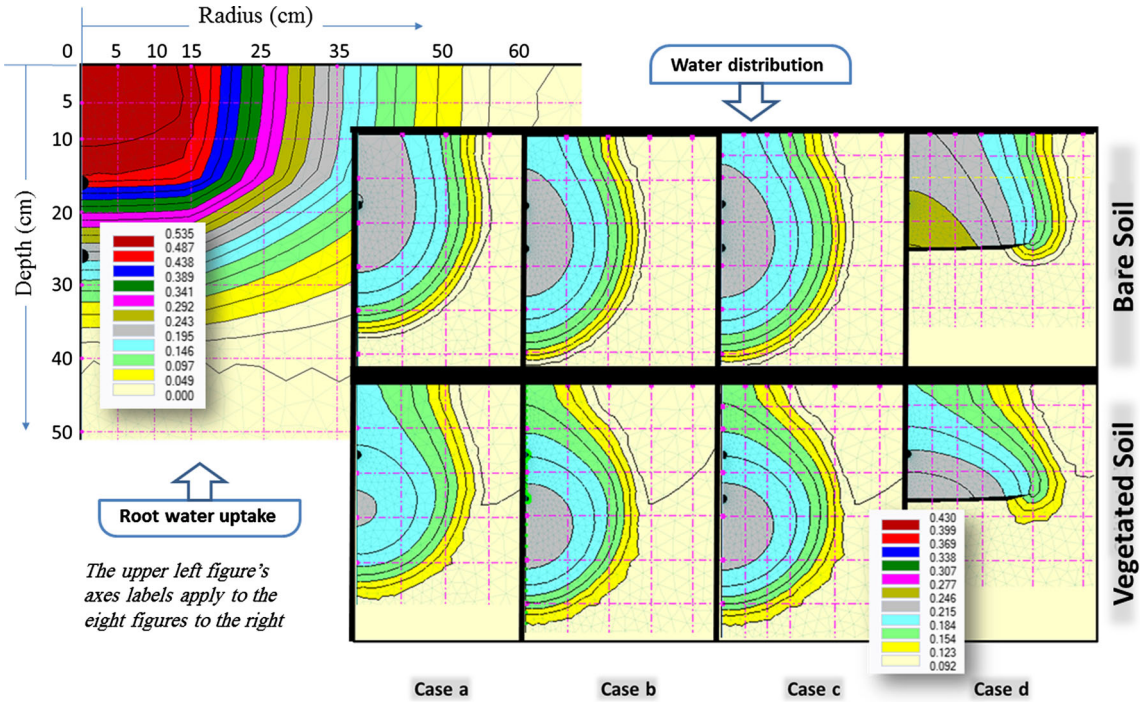

Fig. 11 A comparison of water content distributions for a vegetated soil (*bottom*) and a bare (*top*) loamy soil after 2 days. The *upper left* chart shows the root water uptake pattern for tomato crop

Vegetated soil

All simulations for bare soils discussed above were rerun for soils vegetated with tomatoes and potatoes. Due to the spatial distribution of roots and a corresponding distribution of root water uptake (transpiration) (Fig. 11), crops appear to affect water content distributions mainly in the top layer of the soil profile. The root water uptake pattern of tomatoes, obtained using parameters listed in Table 2, is shown in Fig. 11. Figure 11 shows that the root system takes up water with the highest intensity within a hemisphere with a radius of about 15 cm. This explains the effects the tomato crop has on the water content patterns for the 4 analyzed cases.

Figure 11 compares the water content distributions in the bare (top) and vegetated (bottom) soils at a time of 2,880 min. At that particular time, optimal water contents near field capacity (0.215 cm^3 cm^{-3}) were obtained in almost an entire root zone for case d. This indicates that the frequency of irrigations could be extended to conserve water. Cases b and c are almost identical, showing the least amount of water in the top 30 cm of the soil. Finally, in case a, there is an intermediate amount of water in the root zone, higher than in cases b and c and smaller than in case d. Figure 11 also shows that root water uptake significantly affects the overall distribution of water only in the upper 10–15 cm. Although Fig. 11 only compares results for a bare, loamy soil and a loamy soil vegetated with tomatoes, similar trends were also obtained for a bare, sandy soil and a sandy soil vegetated with potatoes.

Since all simulations only show small changes in water content distributions between the vegetated and bare soils, this allows us to use bare soil simulations in the solute transport simulations discussed next.

Simulation results for solute transport

While water content profiles for scenario with a dual-drip system are different than water content profiles for a scenario with a single dripper, these differences do not seem to be sufficient to explain large differences in reported yields of Jerusalem artichokes (Ismail et al. 2006) and tomatoes and potatoes (ElNesr et al. 2012). Therefore, we have also explored whether the use of a dual-drip system and the presence of a barrier affects solute transport and solute distributions in the root zone. We have rerun many of the simulations discussed above while also considering solute transport. Below, we discuss simulations only carried out for a loamy soil.

Figure 12 shows the distribution patterns of water and solutes for different irrigation scenarios (defined in Fig. 4). In addition to commonly used isolines and spectral maps to present the results for solute concentrations, we also used a new feature that is available in HYDRUS, i.e., the so-called flowing particles. These particles show where a solute

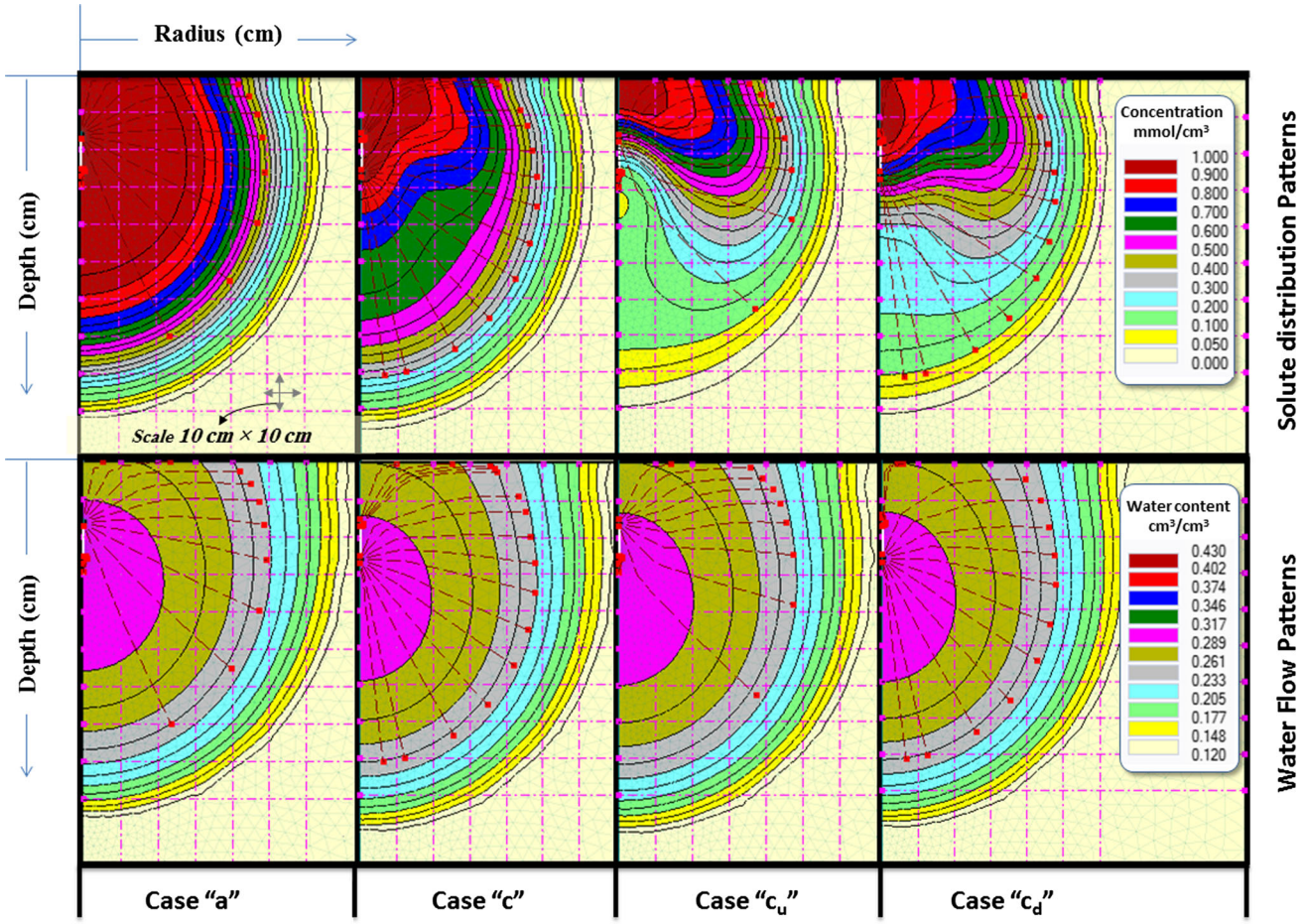

Fig. 12 Water content and concentration distributions at 30 days calculated for different irrigation scenarios for a bare, loamy soil. *Dashed lines* with *red dots* at the end represent flowing particles, indicating flow paths of a non-reactive solute during the infiltration process

particle released at time zero at the boundary of the transport domain (here from the emitter) would be at a particular time, as well as its trajectory. In general, these particles thus visualize the pure convective transport of a nonreactive solute and thus the furthest possible extent of the solute transport from the emitter. While they are not intended to represent any particular fertilizer or a potential crop response, they do provide an indication whether solutes/nutrients will have a tendency to remain in the root zone or, if highly mobile such as nitrates, to leach below the root zone.

While the water content distributions (Fig. 12, bottom) are relatively similar, the concentration patterns are substantially different (Fig. 12, top). Note that in all these scenarios, solute is injected into the transport domain only from the main emitter, while pure water is emitted from the secondary (lower) emitter. When the upper emitter starts operating 120 min before the lower emitter (case c_u), the concentration isolines are pushed upward forcing the solute into the top soil layer and its lateral redistribution, i.e., into the soil layers with the highest density of roots. Only a very small amount of solute leaches downward. On the other hand, when the lower emitter starts operating 120 min (case c_d) before the main emitter, the concentration isolines show a different behavior. The isolines tend to be less compressed than in the former scenario, and a small amount of solute still leaches downward. However, even in this scenario, most solute can be found in the top soil layer and laterally redistributed. Scenario c, with almost concurrent operation of the two emitters, most closely resembles case a with one emitter, although even in this case, the solute bulb is deformed toward upper soil layers.

The effect of the physical barrier on the solute movement is shown in Fig. 13. Figure 13 shows that solute concentrations above the physical barrier are almost equal to the application concentration. This can be beneficial if applied solutes are useful for plants (such as fertilizers) or harmful if applied solutes are damaging to plants (such as emitter-cleaning chemicals or salts). The option to install a physical barrier thus has to be considered from different points of view.

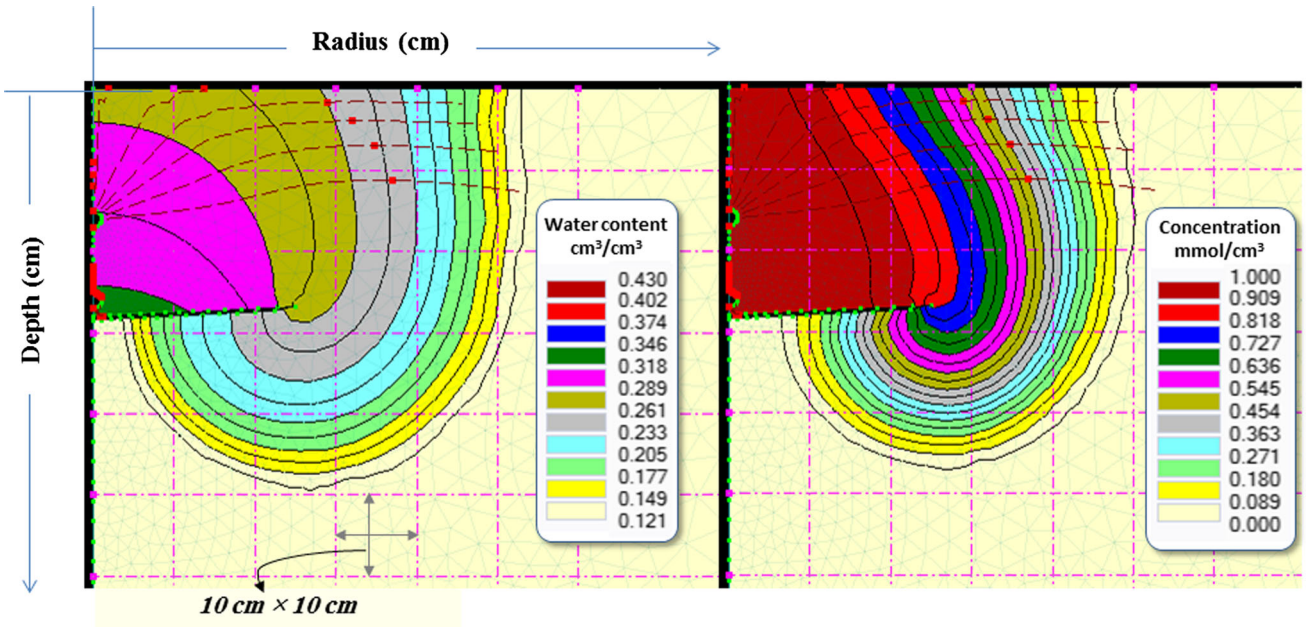

Fig. 13 Water flow and solute transport in the presence of a physical barrier (at 30 days, a bare, loamy soil). *Dashed lines* with *red dots* represent flowing particles (defined in Fig. 12)

Conclusions

Numerical simulations carried out in this study show that the application of a dual-drip system or the installation of a physical barrier can significantly alter both the wetting pattern and spatial distribution of applied solutes. It can be concluded that both the physical barrier and the dual-drip systems are more suitable for the sandy soils than for the loamy soils, as they help solving some of the problems caused by the high infiltration rate in the sandy soils. Physical barriers simply prevent downward movement of all substances (e.g., water, nutrients, and other chemicals), and thus, their usefulness depends on whether we want to retain these substances in the root zone or we prefer to flush them out. A dual-drip irrigation system in addition to improving the redistribution of water applied in sandy soils, it also represents a powerful tool for manipulating the distribution of solutes in the root zone, especially if the two emitters can be operated sequentially. Such a system allows growers to control which solute to retain in the root zone and which one to leach by simply altering the operation of the two drippers. However, this technology requires much more research through the evaluation of larger numbers of possible scenarios involving different solutes, soils, and operation scenarios, especially through evaluation under field conditions.

Acknowledgments The authors wish to express their gratitude to the National Plan of Science and Technology at King Saud University for funding this research by the research project, 10-WAT985-02. Thanks are also due to Alamoudi Chair for Water Research, where this research was being carried out. Many thanks and appreciation are to the associate editor and three anonymous reviewers for their very helpful comments and suggestions.

References

Allen RG, Pereira LS, Raes D, Smith M (1998) Crop evapotranspiration: guidelines for computing crop requirements. Irrigation and drainage Paper No. 56. FAO, Rome

Awady MN, Wassif MA, Abd El-Salam MF, and El-Farrah MA (2008) Moisture distribution from subsurface dripping using saline water in sandy soil. The 15th. Annual Conference of the Misr Society of Ag. Eng., 12–13 March, 2008, pp 477–496

Ayers RS, Westcot DW (1985) Water quality for agriculture. Irrigation and drainage paper No. 29, FAO, Rome

Barth HK (1995) Resource conservation and preservation through a new subsurface irrigation system, In: Lamm FR (ed) Proceedings of the 5th international microirrigation congress, April 2–6, Orlando, FA, ASAE, 168–174

Brandt A, Bresler E, Diner N, Ben-Asher I, Heller J, Goldberg D (1971) Infiltration from a trickle source: I. mathematical model. Soil Sci Soc Am J Proc 35:675–682

Brown KW, Thomas JC, Friedman S, Meiri A (1996) Wetting patterns associated with directed subsurface irrigation. In: Camp CR, Sadler EJ, Yoder RE (eds) Proceedings International Conference on evapotranspiration and irrigation scheduling. St. Joseph, Mich, ASAE, pp 806–811

Carsel RF, Parrish RS (1988) Developing joint probability distributions of soil water retention characteristics. Water Resour Res 24:755–769

Coelho EF, Or D (1999) Root distribution and water uptake patterns of corn under surface and subsurface drip irrigation. Plant Soil 206:123–136

Elawady MN, Abd El, Salam MF, Elnawawy MM, El-Farrah MA (2003) Surface and subsurface irrigation effects on Spinach and sorghum. The 4th Annual Conference of Misr Society of Agricultural Engineers. pp 118–130, Oct 2003

El-Berry AM (1989) Design and utilization of subsurface drip irrigation system for fodder production in arid lands. Misr J Agr Eng 6(2):153–165

ElNesr MN (2011) Subsurface drip irrigation development and modeling of wetting pattern. Lambert Academic Publishing. ISBN-13: 978-3847339106

ElNesr MN, Alazba AA, Amin MT (2012) Assessing the effect of three innovative techniques on water conservation and crop yield through subsurface drip irrigation. Project report, King Saud University

Feddes RA, Kowalik PJ, Zaradny H (1978) Simulation of field water use and crop yield. Wiley, New York, NY

Gärdenäs AI, Hopmans JW, Hanson BR, Šimůnek J (2005) Two-dimensional modeling of nitrate leaching for various fertigation scenarios under micro-irrigation. Agric Water Manag 74(3): 219–242

Hansen VE, Israelsen OW, Stringham GE (1980) Irrigation principles and practices, 4th edn. Wiley, London, p 417

Ismail SM, Zien El-Abedin TK, Wassif MM, El-Nesr MN (2006) Physical and hydraulic barriers under surface and subsurface drip irrigation systems. In: The 14th annual conference of Misr J Agr Eng MSAE, 23(4):1021–1034

Ityel E, Lazarovitch N, Silberbush M, Ben-Gal A (2010) An artificial capillary barrier to improve root zone conditions for horticultural crops: physical effects on water content. Irrig Sci 29(2):171–180. doi:10.1007/s00271-010-0227-3

Ityel E, Lazarovitch N, Silberbush M, Ben-Gal A (2011) An artificial capillary barrier to improve root-zone conditions for horticultural crops: response of pepper, lettuce, melon, and tomato. Irrig Sci 30(4):293–301. doi:10.1007/s00271-011-0281-5

Kampf M, Holfelder T, Montenegro H (1998) Inspection and numerical simulations of flow processes in capillary barrier cover systems. In: Holz KP, Bechteler W, Wang SSY, Kawahara M (eds) Advances in hydro-science and engineering, proceedings of the 3rd international conference on hydro-science and -engineering. Brandenburg University, Cottbus

Kandelous MM, Šimůnek J (2010a) Comparison of numerical, analytical, and empirical models to estimate wetting patterns for surface and subsurface drip irrigation. Irrig Sci 28(5): 435–444

Kandelous MM, Šimůnek J (2010b) Numerical simulations of water movement in a subsurface drip irrigation system under field and laboratory conditions using HYDRUS-2D. Agric Water Manag 97:1070–1076

Kandelous MM, Šimůnek J, van Genuchten MTh, Malek K (2011) Soil water content distributions between two emitters of a subsurface drip irrigation system. Soil Sci Soc Am J 75(2): 488–497

Khalifa HE, El-Gindy AM, Sharaf GA, Allam KhA (2004) Simulating water movement in sandy soil under surface point source emitter, I. model development. Misr J Ag Eng 21(2):341–361

Lazarovitch N, Šimůnek J, Shani U (2005) System dependent boundary condition for water flow from subsurface source. Soil Sci Soc Am J 69(1):46–50

Majumdar DK (2004) Irrigation water management: principles and practice. PHI Learning Pvt. Ltd, New Delhi

Morris CE, Stormont JC (1998) Evaluation of numerical simulations of capillary barrier field tests. Geotech Geolog Eng 16:201–213

Mualem Y (1976) A new model for predicting the hydraulic conductivity of unsaturated porous media. Water Resour Res 12(3):513–522

Phene CJ, Davis KR, Hutmacher RB, McCormick RL (1987) Advantages of subsurface drip irrigation for processing tomatoes. Acta Hortic 200:101–113

Provenzano G (2007) Using HYDRUS-2D simulation model to evaluate wetted soil volume in subsurface drip irrigation systems. J Irrig Drain Eng 133:342–349

Radcliffe D, Šimůnek J (2010) Soil physics with HYDRUS: modeling and applications, CRC Press. Taylor and Francis Group, Boca Raton, FL, p 373. ISBN 978-1-4200-7380-5

Ramos TB, Šimůnek J, Gonçalves MC, Martins JC, Prazeres A, Pereira LS (2012) Two-dimensional modeling of water and nitrogen fate from sweet sorghum irrigated with fresh and blended saline waters. Agric Water Manag 111:87–104

Reich D, Godin R, Chavez JL, Broner I (2009) Subsurface drip irrigation (SDI). Fort collins: Colorado State University. http://www.ext.colostate.edu/pubs/crops/04716.pdf. Accessed: 25.08.2013

Revol PB, Clothier E, Mailhol JC, Vachaud G, Vauclin M (1997) Infiltration from a surface point source and drip irrigation: 2. an approximate time-dependent solution for wet front position. Wat Resour Res 33(8):1869–1874

Šimůnek J, van Genuchten MTh, Šejna M (2008) Development and applications of the HYDRUS and STANMOD software packages, and related codes. Vadose Zone J 7(2):587–600

Šimůnek J, van Genuchten MTh, Šejna M (2011) The HYDRUS software package for simulating two- and three-dimensional movement of water, heat, and multiple solutes in variably-saturated media, technical manual, version 2.0, PC progress, Prague, Czech Republic, pp 258

Singh DK, Rajput TBS, Singh DK, Sikarwar HS, Sahoo RN, Ahmad T (2006) Simulation of soil wetting pattern with subsurface drip irrigation from line source. Agric Water Manag 83(1–2): 130–134

Skaggs TH, Trout TJ, Šimůnek J, Shouse PJ (2004) Comparison of HYDRUS-2D simulations of drip irrigation with experimental observations. J Irrig Drain Eng 130:304–310

Subbaiah R (2013) A review of models for predicting soil water dynamics during trickle irrigation. Irrig Sci 31(3):225–258. doi:10.1007/s00271-011-0309-x

van Genuchten MTh (1980) A closed-form equation for predicting the hydraulic conductivity of unsaturated soils. Soil Sci Soc Am J 44:892–898

Vrugt JA, van Wijk MT, Hopmans JW, Šimůnek J (2001) One-, two-, and three-dimensional root water uptake functions for transient modeling. Water Resour Res 37(10):2457–2470

Warrick AW (1985) Point and line infiltration calculation of the wetted soil surface. Soil Sci Soc Am J Proc 49:1581–1583

Welsh DF, Kreuter UP, Byles JD (1995) Enhancing subsurface drip irrigation through vector flow. In: Lamm FR (ed) Proceedings of the 5th International Microirrigation Congress, Orlando, FA, ASAE, 2–6 April 1995, pp 688–693

Zhou Q, Kang S, Zhang L, Li F (2007) Comparison of APRI and HYDRUS-2D models to simulate soil water dynamics in a vineyard under alternate partial root zone drip irrigation. Plant Soil 291(1):211–223